Progress In Electromagnetics Research, Vol. 123, 263–277, 2012

COMPOSITE SCATTERING OF SHIP ON SEA SURFACE WITH BREAKING WAVES

M. Zhang[1,*], W. Luo[1], G. Luo[1], C. Wang[2], and H.-C. Yin[2]

[1]School of Science, Xidian University, Xi'an 710071, China

[2]Science and Technology on Electromagnetic Scattering Laboratory, Beijing 100854, China

Abstract—The composite backscattering of the ship model on sea surface is investigated with the spilling breaking waves and ship bow waves. The spilling breakers are approximately modeled with the wedge-like waves, and the ship bow waves are simulated based on the Kelvin model. With the modified four-path model, each scattering component is evaluated with the high frequency approximation methods for the total composite scattering. Due to the volume scattering, the composite scattering at large incidence angles is strongly enhanced by the non-Bragg scattering. The relationship of the composite scattering and the ship motion is analyzed. The numerical results of sea surface scattering agree with the measured data well, and the complex physical mechanism of the low-grazing-angle composite scattering is explicitly evaluated in this paper.

1. INTRODUCTION

The investigation of the composite electromagnetic scattering of the ship on sea surface at large incidence angles is the theoretical base for the target detection and high-resolution radar imaging in sea environments [1–4]. Due to complex sea state and multi-interactions between the isolated target and the sea background, the simulation of the full composite scattering is of difficulty for years [5–8]. Different from the pure numerical methods, the high frequency approximations efficiently provide accurate evaluation and convincing physical insight.

Although the Bragg theory has successfully explained the sea surface scattering in small and moderate incidence angles [7, 9–14], some discrepancies between the predictions and the experiment

Received 8 October 2011, Accepted 20 December 2011, Scheduled 24 December 2011

* Corresponding author: Min Zhang (mzhang@mail.xidian.edu.cn).

observations are still observed. According to the experimental data obtained in different sea environments, it was suggested the super events are closely related to the non-Bragg scattering attributed from the breaking waves [15, 16] The scattering of the one-dimensional (1-D) breaking waves, which was generated with the LONGTANK, was combined with the sea surface [17–20]. Moreover, the non-Bragg scattering was taken into the distributed surface scattering with the whitecap coverage [21]. Since it was observed that the sharp wave crests is wedge-shaped [22, 23], the dihedral wedge was used to approximately simulate the breaking waves. In addition, the geometric parameters on the scattering were discussed with numerical methods [24–26].

Due to the horizontal motion of ships in real sea environment, the breaking bow waves and the ship wakes are generated at the bow and the stern respectively. Although the scattering of the ship wakes has been fully investigated with the SAR (Synthetic Aperture Radar) data [27, 28], the influence of the bow waves on the composite scattering from the ship and sea surface is rarely studied in the literatures.

In this paper, the composite backscattering of ship on sea surface is numerically modeled. The full geometric model of the ship and sea surface with the wedge-like spilling waves and the ship bow waves is described in Section 2. Under the frame of modified four-path model, the scattering of the sea surface with breaking waves, the ship and the bow waves are analyzed in Section 3. Section 4 compares the numerical results with the experimental data and other methods, and evaluates the composite scattering in different conditions. Some conclusions are presented in Section 5.

2. GEOMETRIC MODEL

The wind blowing over the sea surface generates wind-driven sea surface. As the high frequency sea spectral components are fully saturated, the wave breaking occurs on the sea surfaces. The locations and the geometric shapes of the breaking waves are the two key points of the simulation of wave breaking.

Recently, the criterions of the wave breaking are the geometrical criterion, kinematic criterion and dynamic criterion, which can be utilized to locate the breaking point on sea waves. According to the solutions to the hydrodynamic equations, the geometrical criterion is used in this paper. If the slope of the sea surface exceeds 0.586, the sea wave is broken.

The evolution of the wave breaking is sorted into three stages: plunging breakers, spilling breakers and surging breakers. As the

spilling breakers is sharply steepened and does not contain the air, this paper use the spilling ones to simulate the typical complex sea surfaces. For the sake of simplicity, it is assumed that all the breakers on the sea surface are in spilling stage. According to the measured sea clutter and photographs in experiments, the spilling ones are approximately simulated with the dihedral wedges of finite length shown in Figure 1. The dihedral wedge is characterized by the internal angle β, length d, width $2l$ and height h, and the validation of the approximation has been proved [29].

Strong ship waves are generated near the bow and stern of moving ships on sea surface. Generally the breaking initiates in the form of a large plunging jet that originates as a sheet of water, climbing up the hull just aft the stern. The energy, which is supplied by the engine of the ship, is converted from the mean flow into energy in the turbulent flow in the wakes by the breakers [30].

Lord Kelvin assumed that the ship is an ideal disturbance source, and modeled the ship wave with divergent and transverse waves [31]. When the ship moves along the $-x$ axis, the ship waves propagate and diffuse along the x axis. The Kelvin ship waves are expressed with the superposition of the plane wave

$$\zeta_K(x,y)=\mathrm{Re}\left\{\int_{-\pi/2}^{\pi/2}F(\phi)\exp\left[-jk_K\sec^2(\phi)(x\cos(\phi)+y\sin(\phi))\right]d\phi\right\} \quad (1)$$

k_K is the wavenumber and ϕ is the angle between the edge of ship waves and x axis. $F(\phi)$ is the characteristic parameter of the ship, which is a complex number. For the sake of simplicity, the thin ship model is used as shown in Figure 2. $F(\phi)$ is expressed as

$$F(\phi)=\frac{2k_K}{\pi}\sec^2(\phi)\iint\frac{\partial Y(x,z)}{\partial x}\exp\left(k_Kz\sec^2(\phi)+k_Kx\sec(\phi)\right)dxdz \quad (2)$$

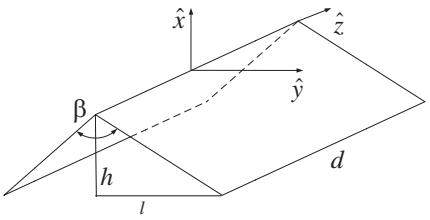

Figure 1. Wedge-shaped spilling breaker.

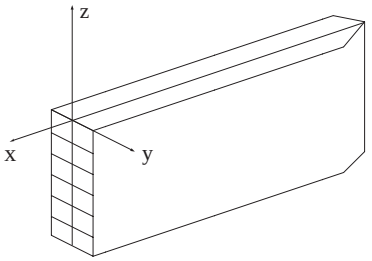

Figure 2. The model of a thin ship.

$$Y(x,z) = \begin{cases} B\left(1 - x^2/L^2\right) & -D \le z \le 0, \quad -L < x < L \\ 0 & z < -D \end{cases} \tag{3}$$

$Y\,(x,\,z)$ is the shape of the water line on the ship. B and L are the half ship width and half ship length respectively. D is the draft of the ship. The amplitudes and phases of the wave components along the ϕ direction are given with $F\,(\phi)$. With Equations (2) and (3), Equation (1) is rewritten as

$$\zeta_K(x,y) = \zeta_{K_0}(x-L,y) + f\zeta_{K_0}(x+L,y) \tag{4}$$

$$\zeta_{K_0}(x,y) = \frac{4B}{\pi k_K L}\int_{-\pi/2}^{\pi/2}\left[1-\exp\left(-k_K D\sec^2(\phi)\right)\right] \sin\left[k_K\sec^2(\phi)(x\cos(\phi)+y\sin(\phi))\right]d\phi \tag{5}$$

The Kelvin ship wave $\zeta_K\,(x,\,y)$ is divided into bow wave $\zeta_{K_0}\,(x-L,\,y)$ and stern wave $\zeta_{K_0}\,(x+L,\,y)$, and f is the viscosity coefficient.

As shown in Figure 3, the Kelvin ship waves are modeled with thin ships. We build the sea surface with the spilling breakers and the ship bow waves firstly, the details of the model meet Ref. [29], here the scale grid of surface is set to $1\times1\,\mathrm{m}^2$ and the sea surface area is $100\times100\,\mathrm{m}^2$. k_i is the incidence direction of the incident electromagnetic wave. The shape parameters of the ship are $B=1\,\mathrm{m}$, $L=5\,\mathrm{m}$ and $D=4\,\mathrm{m}$. The motion speed of ship is $v_s=10\,\mathrm{m/s}$. It is found that the fluctuation of the ship wave is much higher and more regular than the one of calm sea surface. Since the key issue of this paper is the composite scattering of ship and sea waves, only the ship bow wave $\zeta_{K_0}\,(x-L,\,y)$ is considered.

Combined with the spilling breakers and the ship bow waves, the complex ship-sea geometric model is fully established. Different from

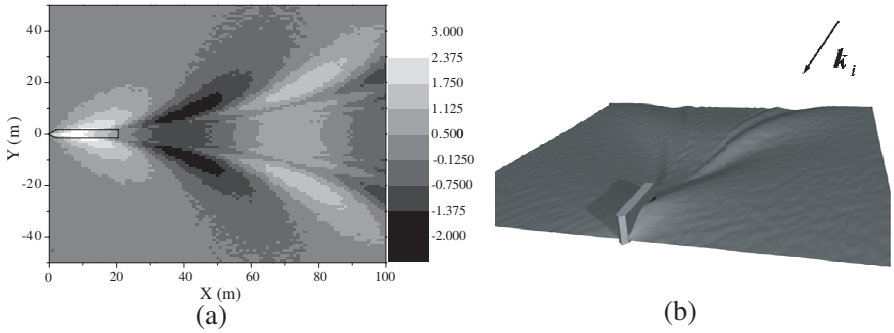

Figure 3. The Kelvin ship wave generated by the thin ship. (a) Gray image of ship wave (unit: m). (b) Three-dimensional fluctuation of ship wave.

the previous ship-sea model, this new model includes the interaction between the ship and the sea waves, which is of significance for the composite scattering in large incidence angles. Once the geometric model is established, we could use the four-path model based on image theory to analyze the composite scattering mechanism of ship on sea surface in high frequency bands as following.

3. COMPOSITE BACKSCATTERING MODEL

For the sake of the complex scattering mechanism of ship on sea surface, the composite scattering is considered as a multi-path scattering mechanism in high electromagnetic frequency bands. The four-path model based on image theory can be adopted to analyze this process. The electric scattering field is usually expressed as four scattering paths

$$\mathbf{E}^{sc} = \mathbf{E}_t + \mathbf{E}_{ts} + \mathbf{E}_{st} + \mathbf{E}_{sts} \tag{6}$$

With the method of equivalent currents (MEC), the direct scattering field $\mathbf{E}_t$ of the target is represented as

$$\begin{aligned} \mathbf{E}_t =& \sum_{i=1}^{N} \mathbf{E}_i^{\text{wedge}} \\ \mathbf{E}^{\text{wedge}} =& jk_0 \int_C \left[\eta_0 I\left(\mathbf{r}'\right) \hat{k}_s \times (\hat{k}_s \times \hat{t}) + M\left(\mathbf{r}'\right) (\hat{k}_s \times \hat{t}) \right] \frac{\exp(-jk_0 s)}{4\pi s} dl \end{aligned} \tag{7}$$

$\mathbf{E}_t$ is the summation of the scattering field $\mathbf{E}^{\text{wedge}}$ of the wedges which constitute the geometrical target model. I and M, which are the equivalent edge electrical current and magnetic current (EEC) flowing along the edge, has three major types [32] and k_0, η_0, $\vec{k}_s$ indicate the wave number of incident wave, the vacuum wave impedance and the unit vector of the scattering wave. $\hat{t}$ and $\vec{r'}$ donate the tangent unit vector on the edge of the surface and the position vector of the edge point. s is the distance from the wedge to the radar receiver, and dl is the line element on the edge of the surface C. The equivalent edge currents for geometrical theory of diffraction (GTDEEC) which involves both the diffraction and reflection fields is chosen in this paper.

According to the image theory, $\mathbf{E}_{ts}$, $\mathbf{E}_{st}$ and $\mathbf{E}_{sts}$, are regarded as the target bistatic scattered fields for corresponding paths with the sea surface reflection coefficients in this paper. The coupling scattering field includes the coherent component in the specular direction of the multiple scattering paths. Since the Fresnel reflection coefficients only represent the specular scattering, a damped reflection coefficient ξ and an extra random phase shift ϕ are introduced to include the

roughness of the sea surface. Then the modified reflection coefficients are expressed as

$$\Gamma_{\perp,\parallel} = \eta R_{\perp,\parallel} \exp(j\phi) \tag{8}$$

$$\eta = \exp\left(-2(k\sigma\cos\theta_i)^2\right), \quad \phi = 2k\zeta(\mathbf{r})\cos\theta_i \tag{9}$$

where the $R_\perp$ and $R_\parallel$ are the Fresnel reflection coefficients, k is the electromagnetic wave number in the free space and θ_i is the incidence angle. σ is the root mean square (RMS) height of the sea surface and $\zeta(\mathbf{r})$ is the undulating height of the sea surface at the reflection point.

In the realistic ocean environment, the sea clutter has significant influence on the composite scattering. With the addition of the sea scattering field $\mathbf{E}_s$, the four-path model is modified as

$$\mathbf{E}^{scs} = \mathbf{E}_t + \mathbf{E}_{ts} + \mathbf{E}_{st} + \mathbf{E}_{sts} + \mathbf{E}_s \tag{10}$$

The two-scale model (TSM) [33], which reckons that the waves contributing to the Bragg process are locally tilted by large-scale waves, is widely used to calculate sea scattering. The classical TSM are used to calculate the scattering coefficient based on the sea spectrum other than the height fluctuation of the sea surface. In order to obtain sea surface scattering field, the TSM is modified as the facet-based model [34, 35], in which both phase shifts associated with the traveled path distance and the reflection coefficients for each scattering facet are considered

$$E_{pq}^{\mathrm{TSM}} = \frac{1}{M}\frac{1}{N}\sum_{i=1}^{M}\sum_{j=1}^{N}\sqrt{I_{ij}\Delta S}\exp\left(j\phi_{\mathrm{add}}\right) \tag{11}$$

$$I_{ij} = \sigma_{pq}^{\mathrm{SPM}}(\theta_i')\left[1 + z_x(x_m, y_n)\tan\theta_i\right] \tag{12}$$

$$\phi_{\mathrm{add}} = \xi\cdot\varphi_{\max} + (\mathbf{k}_i - \mathbf{k}_s)\cdot\mathbf{r} \tag{13}$$

M and N are the sampling number of the sea surface model. $z_x(x_m, y_n)$ is the slope of the sampling point (x, y) in the x direction. I_{ij} and ΔS are the scattering intensity and area of single facet respectively. $\sigma_{pq}^{\mathrm{SPM}}(\theta_i')$ is the small perturbation method (SPM) solution to the scattering from the small scale. $\varphi_{\max}$ is the maximum of the phase difference in the facet and ξ is a random number between -0.5 and 0.5 ($\xi \in [-1/2, 1/2]$). $\mathbf{r}$ is the location of the facet in the global reference frame and $(\mathbf{k}_i - \mathbf{k}_s)\cdot\mathbf{r}$ presents the phase delay caused by the relative position of the facets.

According to the super events in high-resolution radar observation [15], the classical composite model cannot fully explain the measured sea clutter with the Bragg theory at large incidence angles. The wedge-like spilling breakers located on the sea surfaces are introduced

to account for the non-Bragg scattering, and the volume scattering of finite dihedral wedges is analyzed with the MEC [29].

Different from the spilling breakers on the sea surface, the bow waves are caused by the moving ship. According to Equation (1), the Kelvin bow waves are closely related to the shape and speed of the ship, and are independent of the time term and sea state. Thus, the Kelvin bow waves can be considered as deterministic targets. Since it is apparent that the bow waves are in electromagnetically large size, the MEC is used to evaluated the scattering of simulated ship bow waves.

4. NUMERICAL RESULTS

The phase-modified TSM including the breaking waves is compared with the measured data in Figure 4. The measured data were collected from the moderate incidence angles to the low grazing angles at L band [36]. According to the numerical models of breaking wave [17], the width and the length of the wedge are 10λ and 12λ respectively. The *HH* polarization backscattering coefficients are compared under different wind speed. The wind speed of simulation in this paper is 19 m/s and the frequency is 1228 MHz. The solid line indicates the TSM with breakers scattering component, and the dashed line indicates the tilting modified Bragg scattering. The discrete symbols are the measured data under different wind speeds. It is observed that the discrepancy between the classical TSM and the modified one is unconspicuous in moderate incidence angles. While the under-prediction of Bragg scattering in large incidence angles is apparent, the significantly enhanced backscattering is found from the modified

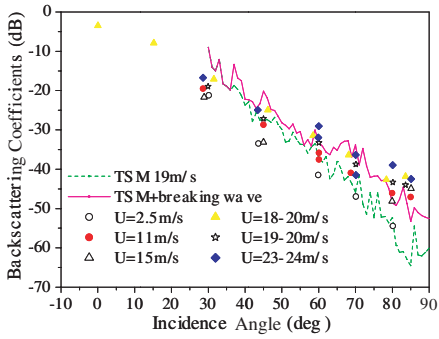

Figure 4. Comparison of the TSM and wedge scattering with the measured data.

TSM with breakers in low grazing angles. In addition, the simulated backscattering coefficients are compared with the experiment data of $U = 18 - 20\,\mathrm{m/s}$ detailed and the mean absolute percentage error (MAPE) is calculated. For moderate incidence angles ($30 \sim 60\,\mathrm{deg}$), the MAPE of TSM is 10.26%, while the MAPE of TSM + breaking wave is 10.95%; for large incidence angles ($60 \sim 90\,\mathrm{deg}$), the MAPE of TSM is 27.79% and the MAPE of TSM + breaking wave is 5.39%, which indicates the method of TSM + breaking wave is better than TSM for large incidence angles, and the parameters of the wedge prove to be reasonable for the agreements of the composite model with the measured data.

The classical TSM and the modified TSM with breaking wave are compared under different wind speeds in Figure 5. The incidence electromagnetic wave is 10 GHz, and both the *VV* and *HH* polarizations are considered. It is noted that the increment of the *HH* polarization is much larger than the one of *VV* counterpart. At

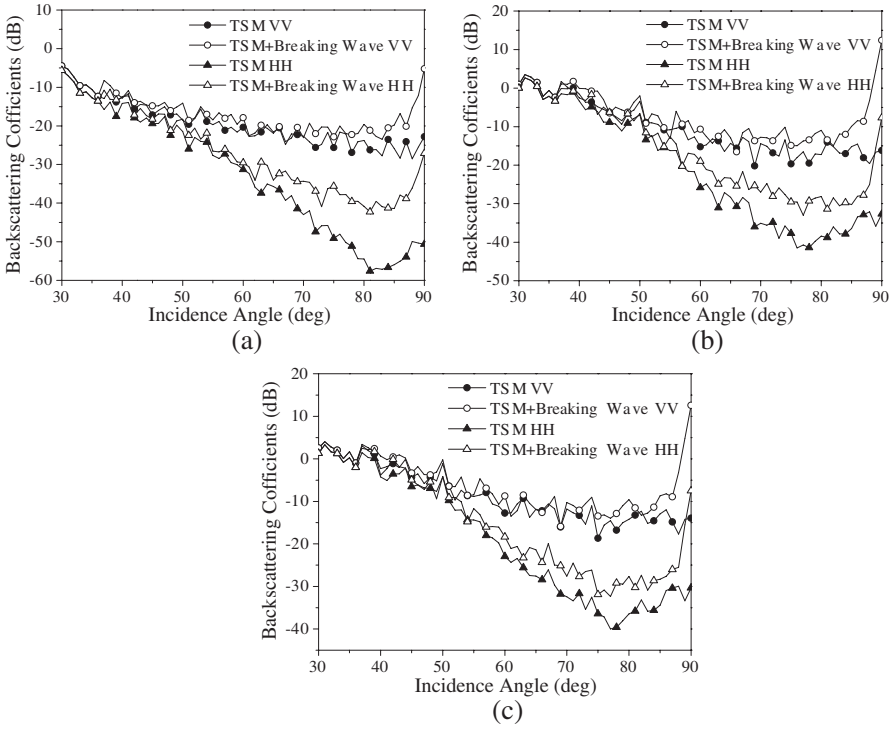

Figure 5. Comparison of the classical TSM with modified TSM under different wind speeds. (a) $U = 5\,\mathrm{m/s}$, (b) $U = 15\,\mathrm{m/s}$, (c) $U = 20\,\mathrm{m/s}$.

low grazing angle, the increment of *HH* is more than 10 even 20 dB, while the increment of *VV* is just 3 to 4 dB. Thus the *HH* polarization becomes comparable with the *VV* polarization in special incidence directions, which is referred as polarization independent. With the increasing wind speed, the increment caused by the breaking waves is weakened. This indicates that the roughness of the sea surface is enhanced by the wind, which increases the randomness of the sea surface fluctuation.

The radar cross section (RCS) of the ship bow waves is evaluated in Figures 6 and 7. The ship width keeps 2 m, and the frequency of the incidence electromagnetic wave is 14 GHz. The comparisons in Figures 6 and 7 show that the *HH* polarized scattering intensity is weaker than the *VV* polarized one, and the average scattering intensity of the *VV* polarized and *HH* polarized are listed in Table 1.

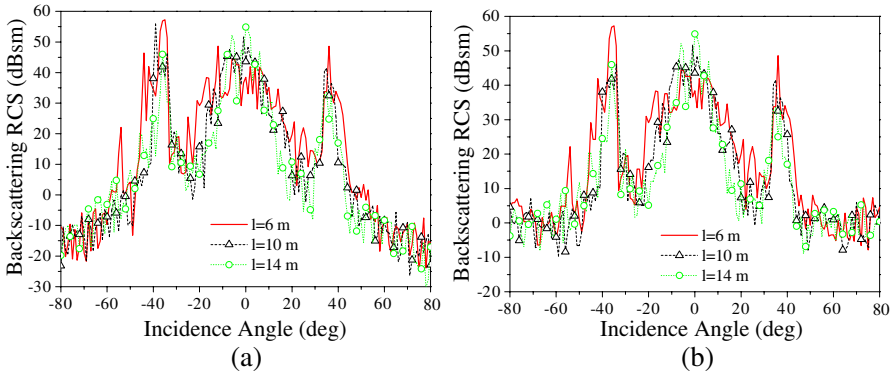

Figure 6. The influence of the ship length on the backscattering RCS of the bow waves. (a) *HH* polarization, (b) *VV* polarization.

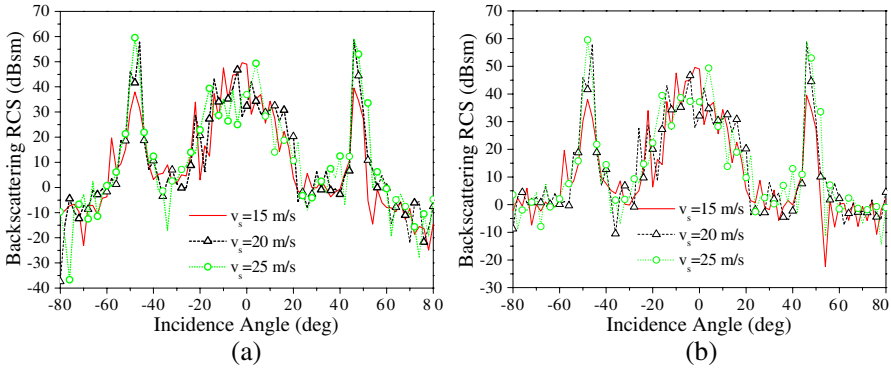

Figure 7. The influence of the ship speed on the backscattering RCS of the bow waves. (a) *HH* polarization, (b) *VV* polarization.

Table 1. The mean values of the RCS in Figures 6 and 7.

Figure 6	$l = 6\,\mathrm{m}$	$l = 10\,\mathrm{m}$	$l = 14\,\mathrm{m}$
HH (dB)	12.570	8.747	7.457
VV (dB)	16.831	13.456	12.162
Figure 7	$v = 15\,\mathrm{m/s}$	$v = 20\,\mathrm{m/s}$	$v = 25\,\mathrm{m/s}$
HH (dB)	8.961	10.552	10.990
VV (dB)	11.702	13.603	14.024

Table 2. The mean values of five points near the peak on the left side in Figure 6.

Five points	$l = 6\,\mathrm{m}$	$l = 10\,\mathrm{m}$	$l = 14\,\mathrm{m}$
HH (dB)	51.706	43.325	35.651
VV (dB)	51.716	41.371	36.532

Table 3. The mean values of five points near the peak on the left side in Figure 7.

Three points	$v = 15\,\mathrm{m/s}$	$v = 20\,\mathrm{m/s}$	$v = 25\,\mathrm{m/s}$
HH (dB)	33.325	48.489	49.326
VV (dB)	33.246	48.487	49.302

The strong specular reflection from the bow wave surfaces is observed in the vertical incidence direction and moderate incidence angles. Figure 6 shows that the influence of the ship length on the scattering is unconspicuous, but the peaks of the backscattering RCS decrease with the increment of the ship length, and the mean value of five points near the peak on the left side is in Table 2. It is also found that the scattering from the bow waves is enhanced by the increasing ship speed in Figure 7, and also, the mean value of three points near the peak on the left side is in Table 3.

The components of the composite scattering from the ship on the sea surface are shown in Figure 8, in which both the spilling breakers and the bow waves are included. The ship width and the ship length are 2 m and 20 m respectively. The ship speed is 20 m/s. Different from the backscattering of the sea surface, the two peaks are observed at 45° and 72° incidence angle, which are caused by the scattering component of the bow waves. Moreover, the bow waves lead the oscillation of the backscattering RCS from 50° to 80° incidence angle.

Figure 9(a) shows that the scattering component of the bow waves is weaken by the increment of the ship length (the mean value of eight

points near the peak is in Table 4), which lead to the decrease of the width of the peak of the composite scattering. It is noted that the ship of small size may cause strong composite scattering because of bow waves. Figure 9(b) shows the influence of the ship speed on the composite scattering, and the mean value of nine points near the peak is also in Table 4. It is observed that the peak of the composite scattering apparently increase with the ship speed in 72° incidence angle. The simulated results indicate that the composite scattering is closely related to the ship speed. It is concluded that the analysis of the microwave scattering of ships in sea environment should include the motion feature of the ships.

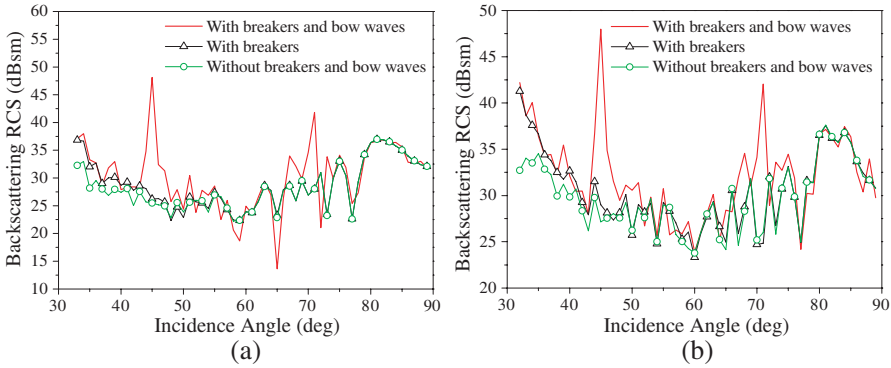

Figure 8. The components of the composite scattering. (a) *HH* polarization, (b) *VV* polarization.

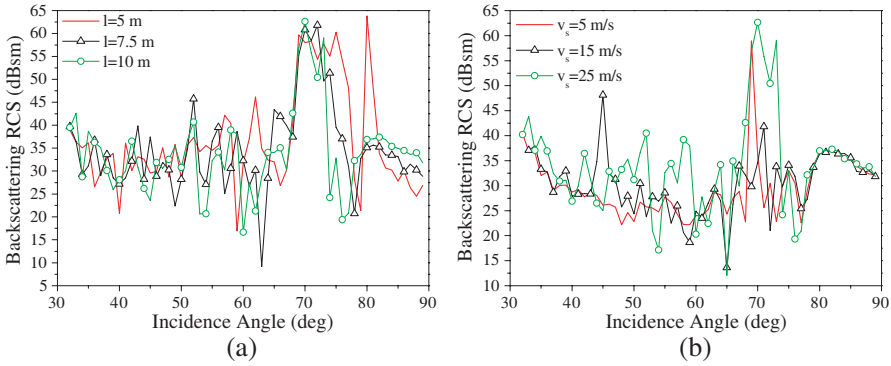

Figure 9. The composite scattering varies with the incidence angles. (a) The influence of ship length on the composite scattering. (b) The influence of ship speed on the composite scattering.

Table 4. The mean value of several points near the peak in Figure 9.

Figure 9(a) Eight points	$l = 5\,\mathrm{m}$	$l = 7.5\,\mathrm{m}$	$l = 10\,\mathrm{m}$
HH (dB)	57.225	51.762	45.158
Figure 9(b) Nine points	$v = 5\,\mathrm{m/s}$	$v = 15\,\mathrm{m/s}$	$v = 25\,\mathrm{m/s}$
HH (dB)	31.433	32.340	46.277

5. CONCLUSION

A modified composite model of ship on sea surface with spilling breakers and ship bow waves is proposed in this paper. The complex breakers are approximately simulated with the finite dihedral wedges, and the breakers are located with the slope criterion. The fair correspondence of the numerical results with the measured data proves the validity of our scattering model. The relationship of the composite scattering and the ship speed is observed in the simulated results, which is apparently different from the previous static composite scattering models. Our study provides refined understanding of the sea clutter, which is helpful for target detection in the open sea environments.

ACKNOWLEDGMENT

The authors would like to thank the anonymous reviewers for their invaluable comments and suggestions, which lead to great improvement of our manuscript, and also thank the National Natural Science Foundation of China under Grant No. 60871070, the Fundamental Research Funds for the Central Universities and the Foundation of the National Electromagnetic Scattering Laboratory to support this kind of research.

REFERENCES

1. Xu, P., K.-S. Chen, and L. Tsang, "Analysis of microwave emission of exponentially correlated rough soil surfaces from 1.4 GHz to 36.5 GHz," *Progress In Electromagnetics Research*, Vol. 108, 205–219, 2010.
2. Liang, D., P. Xu, L. Tsang, Z. Gui, and K.-S. Chen, "Electromagnetic scattering by rough surfaces with large heights and slopes with applications to microwave remote sensing of rough surface over layered media," *Progress In Electromagnetics Research*, Vol. 95, 199–218, 2009.

3. Chen, K.-S., L. Tsang, and J.-C. Shi, "Microwave emission from two-dimensional inhomogeneous dielectric rough surfaces based on physics-based two-grid method," *Progress In Electromagnetics Research*, Vol. 67, 181–203, 2007.
4. Mittal, G. and D. Singh, "Critical analysis of microwave specular scattering response on roughness parameter and moisture content for bare periodic rough surfaces and its retrieval," *Progress In Electromagnetics Research*, Vol. 100, 129–152, 2010.
5. Zhang, M., Y. W. Zhao, H. Chen, and W. Q. Jiang, "SAR imaging simulation for composite model of ship on dynamic ocean scene," *Progress In Electromagnetics Research*, Vol. 113, 395–412, 2011.
6. Luo, W., M. Zhang, Y. W. Zhao, and H. Chen, "An efficient hybrid high-frequency solution for the composite scattering of the ship on very large two-dimensional sea surface," *Progress In Electromagnetics Research M*, Vol. 8, 79–89, 2009.
7. Zhao, Y. W., M. Zhang, and H. Chen, "An efficient ocean SAR raw signal simulation by employing fast fourier transform," *Journal of Electromagnetic Waves and Application*, Vol. 24, No. 16, 2273–2284, 2010.
8. Baussard, A., M. Rochdi, and A. Khenchaf, "PO/Mec-based scattering model for complex objects on a sea surface," *Progress In Electromagnetics Research*, Vol. 111, 229–251, 2011.
9. Brelet, Y. and C. Bourlier, "SPM numerical results from an effective surface impedance for a one-dimensional perfectly-conducting rough sea surface," *Progress In Electromagnetics Research*, Vol. 81, 413–436, 2008.
10. Ishimaru, A., C. Le, Y. Kuga, L. A. Sengers, and T. K. Chan, "Polarimetric scattering theory for high slope rough surface," *Progress In Electromagnetics Research*, Vol. 14, 1–36, 1996.
11. Fabbro, V., C. Bourlier, and P. F. Combes, "Forward propagation modeling above gaussian rough surfaces by the parabolic shadowing effect," *Progress In Electromagnetics Research*, Vol. 58, 243–269, 2006.
12. Yang, W., Z. Zhao, C. Qi, W. Liu, and Z.-P. Nie, "Iterative hybrid method for electromagnetic scattering from a 3-D object above a 2-D random dielectric rough surface," *Progress In Electromagnetics Research*, Vol. 117, 435–448, 2011.
13. Oraizi, H. and S. Hosseinzadeh, "A novel marching algorithm for radio wave propagation modeling over rough surfaces," *Progress In Electromagnetics Research*, Vol. 57, 85–100, 2006.

14. Ji, W.-J. and C.-M. Tong, "Bistatic scattering from two-dimensional dielectric ocean rough surface with a PEC object partially embedded by using the G-Smcg method," *Progress In Electromagnetics Research*, Vol. 105, 119–139, 2010.
15. Lee, P. H. Y., et al., "Wind-speed dependence of small-grazing-angle microwave backscatter from sea surfaces," *IEEE Trans. on Antennas and Propagat.*, Vol. 44, No. 3, 333–340, 1996.
16. Walker, D., "Doppler modelling of radar sea clutter," *IEE Proceedings, Radar, Sonar and Navigation*, Vol. 148, No. 2, 73–80, 2001.
17. West, J. C. and Z. Q. Zhao, "Electromagnetic modeling of multipath scattering from breaking water waves with rough faces," *IEEE Trans. on Geosci. and Remote Sens.*, Vol. 40, No. 3, 583–592, 2002.
18. West, J. C., "Low-grazing-angle (LGA) sea-spike backscattering from plunging breaker crests," *IEEE Trans. on Geosci. and Remote Sens.*, Vol. 40, No. 2, 523–526, 2002.
19. Zhao, Z. Q. and J. C. West, "Low-grazing-angle microwave scattering from a three-dimensional spilling breaker crest: A numerical investigation," *IEEE Trans. on Geosci. and Remote Sens.*, Vol. 43, No. 2, 286–294, 2005.
20. Qi, C., Z. Zhao, W. Yang, Z.-P. Nie, and G. Chen, "Electromagnetic scattering and doppler analysis of three-dimensional breaking wave crests at low-grazing angles," *Progress In Electromagnetics Research*, Vol. 119, 239–252, 2011.
21. Kudryavtsev, V., D. Hauser, G. Caudal, and B. Chapron, "A semiempirical model of the normalized radar cross-section of the sea surface 1. background model," *J. Geophys. Res.*, Vol. 108, No. C3, 8054, 2003.
22. Kalmykov, A. I. and V. V. Pustovoytenko, "On polarization features of radio signals scattered from the sea surface at small grazing angles," *J. Geophys. Res.*, Vol. 81, No. 12, 1960–1964, 1976.
23. Kwoh, D. S. W. and B. M. Lake, "A deterministic, coherent and dual-polarized laboratory study of microwave backscattering from water waves, Part I: Short gravity waves without wind," *IEEE Journal of Oceanic Engineering*, Vol. 9, No. 5, 291–308, 1984.
24. Lyzenga, D. R., A. L. Maffett, and R. A. Shuchman, "The contribution of wedge scattering to the radar cross section of the ocean surface," *IEEE Trans. on Geosci. and Remote Sens.*, Vol. GE-21, No. 4, 502–505, 1983..

25. Ericson, E. A. and D. R. Lyzenga, "Performance of a numerical iterative solution of the surface current integral equation for surfaces containing small radii of curvature," *Radio Sci.*, Vol. 33, No. 2, 205–217, 1998.
26. Lyzenga, D. R. and E. A. Ericson, "Numerical calculations of radar scattering from sharply peaked ocean waves," *IEEE Trans. on Geosci. and Remote Sens.*, Vol. 36, No. 2, 636–646, 1998.
27. Tunaley, J. K. E., E. H. Buller, K. H. Wu, and M. T. Rey, "The simulation of the SAR image of a ship wake," *IEEE Trans. on Geosci. and Remote Sens.*, Vol. 29, No. 1, 149–156, 1991.
28. Ai, J., X. Qi, W. Yu, et al., "A novel ship wake CFAR detection algorithm based on SCR enhancement and normalized hough transform," *IEEE Trans. on Geosci. and Remote Sens.*, Vol. 8, No. 4, 681–685, 2011.
29. Luo, W., M. Zhang, C. Wang, and H.-C. Yin, "Investigation of low-grazing-angle microwave backscattering from 3-D breaking Sea Waves," *Progress In Electromagnetics Research*, Vol. 119, 279–298, 2011.
30. Shakeri, M., M. Tavakolinejad, and J. H. Duncan, "An experimental investigation of divergent bow waves simulated by a two-dimensional plus temporal wave marker technique," *J. Fluid Mech.*, Vol. 634, 217–243, 2009.
31. Hennings, R. R., W. Alpers, and A. Viola, "Radar imaging of kelvin arms of ship wakes," *Int. J. Remote Sensing*, Vol. 20, No. 13, 2519–2543, 1999.
32. Ando, M., T. Murasaki, and T. Kinoshita, "Elimination of false singularities in GTD equivalent edge currents," *IEE Proceedings H Microwaves, Antennas and Propagation*, Vol. 138, 289–296, 1991.
33. Fung, A. K. and K. K. Lee, "A semi-empirical sea-spectrum model for scattering coefficient estimation," *IEEE Journal of Oceanic Engineering*, Vol. 7, 166–176, 1982.
34. Soriano, G., M. Joelson, and M. Saillard, "Doppler spectra from a two-dimensional ocean surface at L-band," *IEEE Trans. on Geosci. and Remote Sens.*, Vol. 44, 2430–2437, 2006.
35. Chen, H., M. Zhang, Y. Zhao, and W. Luo, "An efficient slope-deterministic facet model for SAR imagery simulation of marine scene," *IEEE Trans. on Antennas and Propagat.*, Vol. 58, No. 11, 3751–3756, 2010.
36. Guinard, N. W., J. T. Ransone, and J. C. Daley, "Variation of the NRCS of the sea with increasing roughness," *J. Geophys. Res.*, Vol. 76, 1525–1538, 1971.